Comparison of the Binding and Reactivity of Plant and Mammalian Peroxidases to Indole Derivatives by Computational Docking†

Henrik R. Hallingbäck,‡ Razif R. Gabdoulline,§ and Rebecca C. Wade*,§

Molecular and Cellular Modeling Group, EML Research gGmbH, Schloss-Wolfsbrunnenweg 33, 69118 Heidelberg, Germany, and Molecular Biotechnology Programme, Biomedical Center, Uppsala University School of Engineering, S-75124 Uppsala, Sweden

Received July 29, 2005; Revised Manuscript Received November 16, 2005

ABSTRACT: The oxidation of melatonin by the mammalian myeloperoxidase (MPO) provides protection against the damaging effects of reactive oxygen species. Indole derivatives, such as melatonin and serotonin, are also substrates of the plant horseradish peroxidase (HRP), but this enzyme exhibits remarkable differences from MPO in the specificity and reaction rates for these compounds. A structural understanding of the determinants of the reactivity of these enzymes to indole derivatives would greatly aid their exploitation for biosynthetic and drug design applications. Consequently, after validation of the docking procedure, we performed computational docking of melatonin and serotonin to structural models of the ferric and compound I and II (co I and co II, respectively) states of HRP and MPO. The substrates dock at the heme edge on the distal side, but with different orientations in the two proteins. The distal cavity is larger in MPO than in HRP; however, in MPO, the substrates make closer contacts with the heme involving ring stacking, whereas in HRP, no ring stacking is observed. The observed differences in substrate binding may contribute to the higher reaction rates and lower substrate specificity of MPO relative to those of HRP. The docking results, along with the previously measured heme−protein reduction potentials, suggest that the differentially lowered reaction rates of co II of HRP and MPO with respect to those of co I could stem from as yet undetermined conformational or electrostatic differences between the co I and co II states of MPO, which are absent in HRP.

There are two superfamilies of heme peroxidases (*1*). These have different structural folds as well as different covalent coordinations of the heme cofactor. Superfamily I comprises the bacterial, fungal, and plant peroxidases, whereas the mammalian peroxidases constitute superfamily II. Here, we compare the best characterized representatives of the two superfamilies: horseradish peroxidase (C isoenzyme, HRP)[1] and human myeloperoxidase (MPO). HRP is an important diagnostic marker in molecular biology experiments, and application domains for HRP include organic synthesis, biotransformation, bioremediation, medical diagnostics, and targeted cancer therapy (*2*). MPO is the most abundant protein in the phagosomes of neutrophils and contributes to the immune defense system (*3*, *4*). It has been implicated in diseases such as atherosclerosis, rheumatoid arthritis, cancer, multiple sclerosis, and Alzheimer's disease (*5*) and also contributes to drug metabolism and toxicity (*6*).

Both these peroxidases can oxidize a variety of aromatic compounds, including the indole derivatives, melatonin (*N*-acetyl-5-methoxytryptamine, MLT), and serotonin (5-hydroxytryptamine, SRT), a serum vasoconstrictor and neurotransmitter (see Chart 1). MLT is a hormone synthesized by the pineal gland and is implicated as one of the physiological substrates of MPO (*7*−*9*). It is found in significant concentrations in blood and bone marrow. A regulatory role has been suggested for MLT in an oscillating MPO defense system in the neutrophil (*10*). The oscillations are thought to contribute to the robustness of the white blood cells against the radicals and hyphalous acids that MPO produces to destroy foreign bodies (*11*). For HRP (and other plant peroxidases), an important physiological indole substrate is the auxin, indole-3-acetic acid, the principal promoter of plant growth (*1*).

Reactions with indole derivatives are generally considered to be catalyzed by the peroxidase redox intermediate co I and II states (*1*, *12*) (Figure 1), although there is also evidence for catalysis of MLT by compound III of HRP (*13*). Measurements of the standard redox potentials of the peroxidases (*14*−*16*) show their strong oxidative potential, particularly for the MPO co I/co II couple (Table 1). The bimolecular rate constants for the reactions catalyzed by the co I and co II states (*12*, *17*), k_2 and k_3, respectively, are given in Table 1. All the rate constants for SRT are greater

† This work was supported in part by the Klaus Tschira Foundation and the German Federal Ministry of Education and Research (BMBF Grant 0313076). H.H. was a student of the Molecular Biotechnology Programme, Uppsala University.

* To whom correspondence should be addressed. Telephone: +49 6221 533 247. Fax: +49 6221 533 298. E-mail: rebecca.wade@eml-r.villa-bosch.de.

‡ Uppsala University School of Engineering. Current address: Institute of Plant Biology and Forest Genetics, Swedish University of Agriculture, Box 7080, 750 07 Uppsala, Sweden.

§ EML Research gGmbH.

[1] Abbreviations: BHA, benzhydroxamic acid; co I, compound I; co II, compound II; FER, ferulic acid; HRP, horseradish peroxidase; IAA, indole-3-acetic acid; MLT, melatonin; MPO, myeloperoxidase; rmsd, root-mean-square deviation; SRT, serotonin.

10.1021/bi051510e CCC: $33.50
Published on Web 02/07/2006

Chart 1: Chemical Structures of the Substrates Used in This Study Shown in Standard Protonation States at pH 7.0[a]

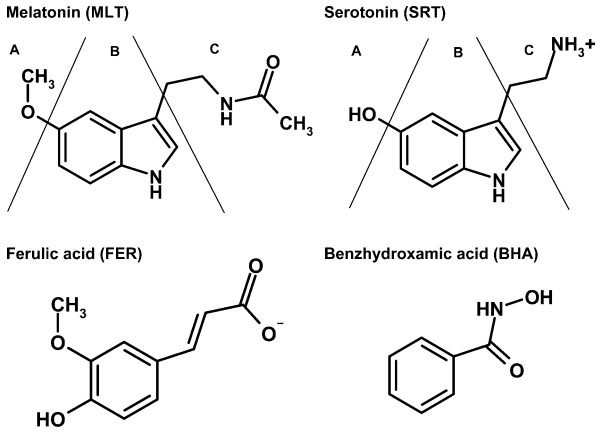

[a] The parts of the indoles are called (A) the indole substituent (IS), (B) the indole ring (I), and (C) the side chain (SC).

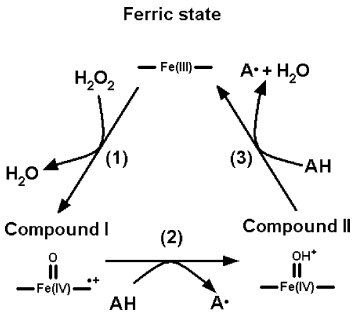

FIGURE 1: Part of the heme peroxidase reaction cycle with oxidation states and reactions (numbered) relevant to this study shown (*1*). The ferric state peroxidase donates two electrons to transform hydrogen peroxide to water and form the redox intermediate compound I, with a ferryl oxygen, an Fe(IV) ion, and a porphyrin π-cation radical (reaction 1) (*12*, *26*, *27*). The co I state peroxidase can oxidize an aromatic substrate (AH) by extracting one electron and one proton from it and transforming it into a radical (A$^{\bullet}$) (reaction 2). This leaves the peroxidase in the co II state, with a proton bound either to the ferryl oxygen (*19*) or to the apoprotein (*12*, *28*) and the porphyrin π-cation radical abolished by the donated electron. Finally, the peroxidase can regain the ferric state from co II by extracting another electron and another proton from an aromatic substrate and transforming it into a radical (reaction 3). MPO, but not HRP, can, additionally, regain the ferric state directly from co I by peroxidation of halide ions to toxic hypohalous acids in a two-electron transfer reduction. This reaction is thought to be the main route by which MPO contributes to the mammalian immune defense system (*1*, *3*).

than those for MLT, consistent with SRT's lower standard redox potential (*12*, *18*), reflecting its ability to act as an excellent electron donor. However, the relative rate constants differ for co I states of HRP and MPO. Although the differences in rate constants for co I and co II of these two enzymes for these two substrates can be related to the redox potentials of the proteins and substrates (Table 1), a full understanding of the basis for differences in reactivity and specificity requires structural models of enzyme−substrate complexes and the determinants of electron transfer events. Indeed, the electron reduction potentials themselves depend on structural properties.

In this paper, we first use probe−protein interaction energy maps to examine the accessibility of the active sites in HRP and MPO. Then, we validate our docking procedure by comparing docking results for benzhydroxamic acid (BHA) and ferulic acid (FER) (see Chart 1) against crystal structures of their complexes with HRP. Finally, we use the docking procedure to derive structural models of MLT and SRT in complex with the ferric, co I, and co II states of HRP and MPO. The docked structures were clustered and classified according to their proximity to the heme edge and the orientation of the ligand. For HRP, these models are based on the crystal structures of the protein in the three oxidation states. For MPO, crystal structures are only available for the ferric form. The co I and co II states of MPO were consequently modeled on the basis of the ferric MPO structure and the known co I and co II HRP structures. This modeling procedure is evaluated by reference to HRP.

In the Discussion, we compare the results of the computations with the experimental rate constants for the reactions of co I and co II, first for the two proteins in general, then for the two substrates, and last for the different protein oxidation states. We find that the larger rate constants and lower substrate specificity of MPO versus those of HRP are consistent with the greater accessibility of the heme edge in MPO than HRP and the fact that docking modes with aromatic stacking are observed in MPO but not in HRP. Comparison of the docked model structures, along with consideration of the known heme−protein reduction potentials, does not however quantitatively explain the relative rates for the reactions of co I and co II for the two proteins. These data suggest that there are as yet undetermined conformational or electrostatic differences between the co I and co II states of MPO that are absent in HRP.

MATERIALS AND METHODS

Preparation of Molecular Coordinates. Crystallographic coordinates with the following PDB identifiers were used. For HRP, 7ATJ (determined with cyanide and ferulic acid bound) (*19*), 1HCH (co I) (*20*), and 1H55 (co II) (*20*) were used. For MPO in all reaction states, the A and C chains from 1D2V (determined with bromide bound) (*4*) were used. These chains make up one monomer of the 140 kDa MPO homodimer; the other monomer was neglected as the active sites are far from the monomer−monomer interface. All nonprotein atoms, except the heme and any calcium ions, were removed before the structures were prepared for the calculations. All protein structures were overlaid by superimposing their protoporphyrin rings. The rmsd values of the superposed porphyrins for each protein were less than 0.2 Å, but the porphyrins were rotated 180° with respect to each other in HRP and MPO to correctly superpose the active sites, including the distal and proximal histidines (see Figure 2), as well as the distal arginine (position 38 in HRP and position 239 in MPO) (*11*).

Co I and co II of MPO were modeled by including the ferryl oxygens of the HRP structures, 1HCH and 1H55, respectively, in the MPO structure. To investigate the effect of structural differences between the different reactive forms, additional models of co I and co II of HRP were also made by superposition of the ferryl oxygens of 1HCH and 1H55, respectively, onto the 7ATJ structure of HRP.

The protonation states of the heme−protein titratable groups were set according to previous pK_a calculations (*11*) for pH 7.

Structural models of MLT and SRT (including hydrogens) were generated with the CORINA webserver (http://

Table 1: Experimental Measurements for the Reaction of Horseradish Peroxidase and Myeloperoxidase with the Substrates Melatonin and Serotonin

		horseradish peroxidase		myeloperoxidase	
substrate	$E^{\circ\prime}_s$[a]	k_2	k_3	k_2	k_3
serotonin	0.65	$(8.1 \pm 0.4) \times 10^6$	$(1.2 \pm 0.1) \times 10^6$	$(1.7 \pm 0.1) \times 10^7$	$(1.4 \pm 0.1) \times 10^6$
melatonin	0.95	$(1.3 \pm 0.1) \times 10^4$	$(5.2 \pm 0.4) \times 10^2$	$(6.1 \pm 0.2) \times 10^6$	$(9.6 \pm 0.3) \times 10^2$
	$E^{\circ\prime}_p$[a]	0.898	0.869	1.35	0.97

[a] Standard single-electron reduction potentials (in volts) are given for the relevant redox couples of the heme proteins ($E^{\circ\prime}_p$) (*14*−*16*) and of the substrates ($E^{\circ\prime}_s$) (*12*, *18*). Bimolecular rate constants (M^{-1} s^{-1}) for reduction of compounds I (k_2) and II (k_3) were measured at pH 7.0 and 25 °C (*12*, *17*).

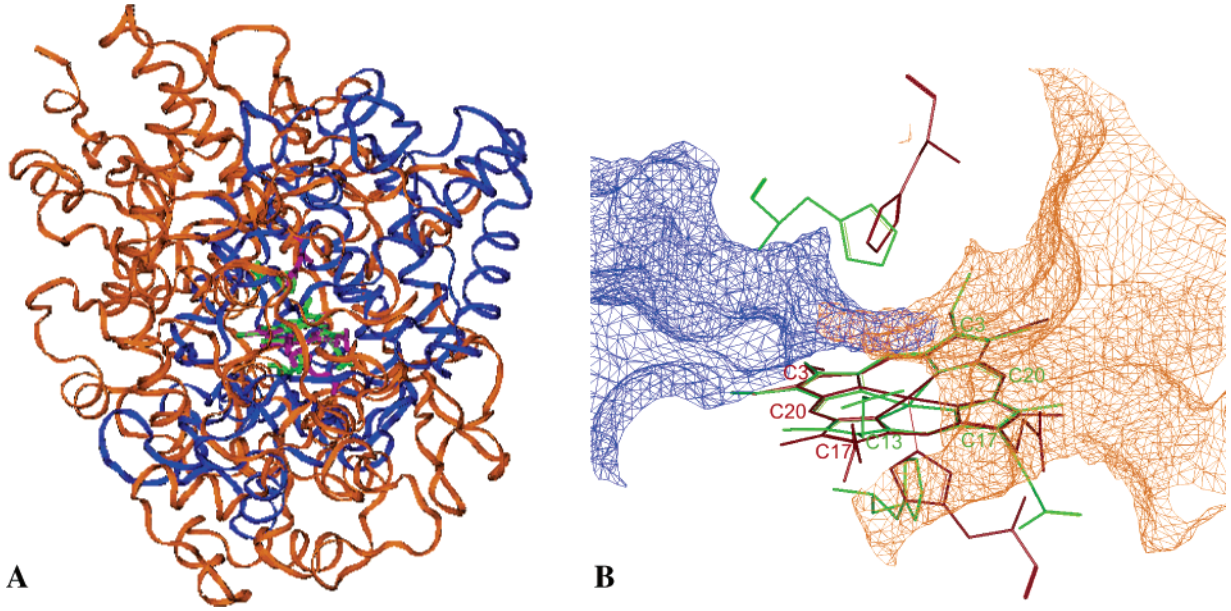

FIGURE 2: Superposition of ferric HRP (blue and purple) and MPO (orange and green). (A) The proteins, shown by their backbone ribbons, have very different crystal structures, which are overlaid by superimposing their active sites. The ferriprotoporphyrin IX prosthetic groups and the proximal and distal histidines are shown in stick representation. In HRP, the heme is stabilized through the coordinating proximal histidine and by nonbonding interactions of the active site. In MPO, however, there are also three covalent bonds between the heme and the apoprotein [C12 methyl (CMD)−Asp A94, C2 methyl (CMB)−Glu C242, and C3 vinyl α-carbon (CAB)−Met C243] (*1*). (B) Close-up of the overlaid active site heme cofactors and distal and proximal histidines from the same view. Energy contours at 0.5 kcal/mol computed with GRID show the regions accessible to a water molecule probe in the proteins. The access channels point in different directions in the two proteins. The MPO heme is rotated 180° with respect to the heme of HRP with the axis of rotation pointing from the Fe ion toward the reader. Selected carbons are labeled in the colors of the respective hemes. (A superposition of the hemes of HRP and MPO, without taking the position of the active site histidines into account, would result in the superposition of the proximal histidine of HRP onto the MPO distal cavity and vice versa.)

www2.chemie.uni-erlangen.de/software/corina/free_struct.html). SRT was modeled with the amino group both protonated (charged) and unprotonated (neutral). Coordinates of BHA and FER (Chart 1) were taken from their complexes with HRP, 1GX2 and 6ATJ, respectively, and hydrogen atoms added using SYBYL version 6.9.1 (http://www.tripos.com). All ligand structures were optimized by fast energy minimization and assigned Gasteiger charges for their protonation state at pH 7 using SYBYL version 6.9.1. All nonpolar hydrogens were then deleted, adding their charges to that of their closest bonded non-hydrogen atom (united-atom principle) (see the Supporting Information).

GRID Calculations. GRID version 21 (www.moldiscovery.com) (*21*) was used to compute probe−target interaction energies to map out and compare the potential binding interactions of the protein binding sites. Partial atomic charges for the heme were assigned according to scheme A (*22*) described in the Supporting Information. All other parameters were assigned from the GRID parameter set. The grid for probe−target interaction energy computations encompassed the active site and the channel to the active site. The grids for HRP had dimensions of 30 Å × 20 Å × 20 Å and those for MPO dimensions of 20 Å × 35 Å × 30 Å. The grid spacing was 0.5 Å. The probes were chosen to represent the functional groups in MLT and SRT and included water (OH2), hydrophobic (DRY), methyl (C3), carboxyl oxygen (O::), and protonated amino (NH_3^+) probes.

AUTODOCK Calculations. AUTODOCK version 3.0 (*23*) was used to dock ligands into the protein binding sites. All single bonds in the ligands, except amide and peptide bonds, were considered rotatable. The number of rotatable bonds was four in MLT, SRT, and FER and two in BHA.

Polar hydrogens were added to the protein structures using WHATIF version 5.0 (*24*), subject to constraints to maintain the previously assigned protonation state (*11*). In HRP, the distal His 42 was protonated on the $N^{\delta 1}$ atom and constrained to disallow side chain rotation. In MPO, the distal His A95 was protonated on the $N^{\delta 1}$ atom and constrained to disallow side chain rotation, and Asp A98 was protonated on the $O^{\delta 2}$ atom.

The heme Fe ion and its coordinating nitrogens were assigned "independent" atom types as recommended in the

AUTODOCK manual, and the recommended Fe atom parameters were used (see http://www.scripps.edu/mb/olson/doc/autodock/). As AUTODOCK cannot handle more than seven atom types, the calcium ions were assumed to have the same repulsion/dispersion properties as the Fe ion. Other parameters were assigned default values (*23*).

Kollman united-atom charges were applied to the protein. Heme charges were assigned according to scheme B (*22*, *25*, *27*) as described in the Supporting Information. Calcium ions were assigned the formal charge of +2e. When an additional CN^- ion and a water molecule were present in the active site, the charges on the CN^- ion were assigned as Gasteiger type using SYBYL version 6.9.1, and the charges for the water molecule were obtained from the GRID parameter set.

The grid for probe−target interaction energy computations encompassed the active site and the channel to the active site. The grids for HRP had dimensions of 30 Å × 20 Å × 20 Å and those for MPO dimensions of 20 Å × 35 Å × 30 Å. Grids were calculated for all atom types present in the ligands: C, aliphatic carbon; A, aromatic carbon; N, nitrogen; O, oxygen; and H, polar hydrogen.

For each ligand docking, 50 runs with the Lamarckian genetic algorithm having 50 individuals in the population were made. For each run, the maximum number of generations and of energy evaluations was set at 27 000 and 1.0×10^6, respectively. The number of individuals that could survive by elitism was set at 1, and the number of generations to pick the worst individual (*N*) was set at 10. All other parameters were set to default values (*23*), and every simulation was repeated once with the same parameters but a different random seed. The resulting 50 + 50 docking solutions were subsequently clustered with AUTODOCK Tools, both separately and together to control for adequate sampling.

The lowest-energy pose in a cluster was designated the cluster representative and its docking energy the cluster energy. The cluster strength is the percentage of the total number of resultant conformations belonging to the cluster at a particular value of the clustering rmsd tolerance threshold (R_{tol}). R_{tol} was set at 1.0 Å. A second clustering with an R_{tol} of 0.2 Å was performed to ensure that the representative of each 1.0 Å cluster was not an outlier within that cluster. To designate a cluster as significant, it was required to have a strength of at least 6% in both of the docking runs and to have structurally similar cluster representatives differing in cluster energy by less than 0.05 kcal/mol. Thereafter, the results of both docking runs were clustered together, and the (merged) significant clusters defined the modes.

Mode representative, mode energy, and mode strength were then defined analogously with respect to the terms for clusters. To measure the reproducibility of the simulation, the mode strength percentages were summed to make up the total mode strength. Conformations not in modes either are outliers or belong to clusters that were not reproduced well enough to make them significant. If the total mode strength was very low (<50% with $R_{tol} = 1.0$ Å), the simulation was not considered to be reproducible and had to be reparametrized. Modes were identified using an R_{tol} of 1.0 Å, but in some cases, modes or submodes were also identified using smaller values of R_{tol}. Modes were classified according to which part of the ligand points to the distal cavity and heme as IS (indole substituent), I (indole ring), or SC (side chain) (see Chart 1). Each mode thus represents a distinct binding arrangement of the ligand in the protein binding site that was identified through (spatial) clustering of the lowest-energy structures recorded in two AUTODOCK runs.

RESULTS

Probe Accessibility of the Active Sites of HRP and MPO. The shape and orientation of the channel from the surface to the active site are different in HRP and MPO. This is illustrated by the surface accessible to a water probe computed with the GRID program (see Figure 2). The channels originate from nearly opposite directions. Nevertheless, as a consequence of the heme of MPO being rotated 180° compared to that in HRP, the channels pass over the C20 atom at the heme edge in both MPO and HRP. The probes can venture further into the distal cavity of MPO than into that of HRP. The sixth ligand position above the ferric ion was accessible (according to the criterion of an interaction energy of <0.5 kcal/mol) to all the GRID probes tested in MPO, but this position was not accessible to the protonated amino group in HRP.

The GRID energy maps also indicate different approach routes to the heme edge in the two enzymes. In HRP, there is a rather narrow channel (blue contours in Figure 2B) to the heme lying in the proximity of the C20 atom and closer to the C17 propionate side than to the C3 vinyl side. The volume enclosed by the solvent accessible molecular surface of this channel is 1445 $Å^3$ [as computed with the CASTp server (http://cast.engr.uic.edu/cast/) (*33*)]. In contrast, in MPO, the energy maps (orange contours in Figure 2B) show a larger probe contact surface with the heme edge. The volume enclosed by the solvent accessible molecular surface of this channel is 2505 $Å^3$. The water probe can reside directly above the D ring and over the C17 propionate. Note that this propionate is directed toward the proximal side of the active site in contrast to the MPO C13 propionate and to both HRP propionates, which are directed to the distal side and prohibit probes or substrates from entering this region. This orientation of the MPO C17 propionate is observed not only in the 1D2V crystal structure but also in other crystal structures of MPO [PDB entries 1CXP (*4*) and 1DNW (*32*)].

The GRID maps for HRP structures in co I and co II states were very similar to each other and differed from those for the ferric HRP only near the sixth ligand position. While the sixth ligand position was accessible to a carboxyl oxygen probe, for example, in the ferric HRP, it was sterically occluded by the ferryl oxygen in co I and co II, and the region accessible to this probe only extended over the heme edge and beyond the C20 atom by approximately 1 Å. These observations fit with the proposal that reactions 2 and 3, which require larger aromatic substrates, take place at the heme edge.

Validation of the Docking Procedure. The GRID maps permit the binding possibilities of the proteins to be assessed and compared for a range of functional group probes with a detailed empirical energy function including hydrogen bond directionality. To dock complete molecules into the protein binding sites, accounting for their flexibility, it was necessary to use another program. We chose to use AUTODOCK for

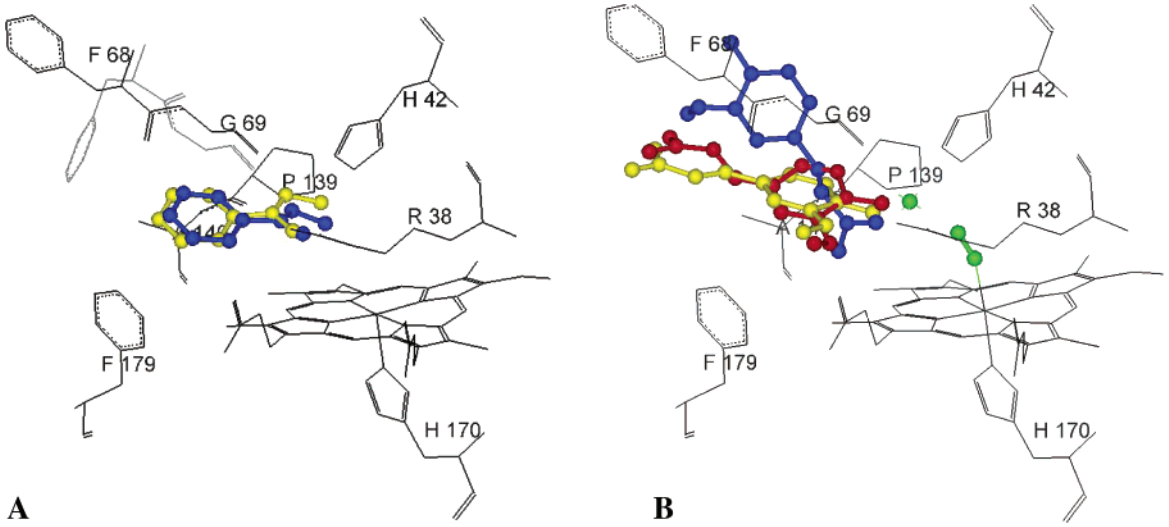

FIGURE 3: (A) Highest-strength docking mode (blue) of BHA docked to ferric HRP closely matches, with a rmsd of 0.6 Å, the BHA ligand (yellow) in the crystal structure. The binding of BHA has been shown to induce Phe 68 to form a "lid" over the substrate (see the part of structure 1GX2 shown in gray but not used for docking). (B) The two best scored docked modes of FER to ferric HRP with a CN^- ion (green) present as the sixth Fe-coordinating ligand and a water molecule (green) included as part of the target. The FA1 mode (yellow) was observed in the crystallographic structure with the CN^- ion present. The rmsds of the best (blue) and second best scored docked modes (red) to FA1 are 6.3 and 0.9 Å, respectively (see the text).

this purpose. Like GRID, AUTODOCK first maps the binding site to a grid and computes the interactions of different atom types with the target at the grid points. It then uses a genetic algorithm to dock the ligand on the grid under the consideration of atom-specific interactions and the ligand's rotational degrees of freedom. Both GRID and AUTODOCK are widely used and have been shown to be able to reproduce experimentally observed binding arrangements for a variety of protein targets, including heme proteins. However, docking programs generally yield correctly docked ligand structures only ~70−80% of the time (*34*). Therefore, to assess the reliability of the ligand docking procedure, including our procedure for clustering of the docking poses, we have docked into HRP two aromatic substrates, BHA and FER, whose crystal structures in complex with HRP are available (*19*, *28*). Of the crystal structures available, these are the most relevant for the docking problem addressed in this paper: no crystal structures of MPO−substrate complexes or of HRP−indole derivative complexes have been determined.

Benzhydroxamic acid (BHA) is a substrate of reactions 2 and 3 of HRP, and its structure in complex with ferric HRP has been determined (*28*). Once docking to the ferric HRP structure (7ATJ, which was determined in the presence of ferulic acid, not BHA) had taken place, two docking modes were detected, with similar energy scores of −7.3 and −6.9 kcal/mol. The latter mode was the most populated and reproduced the position of BHA in the crystal structure of the ferric HRP−BHA complex (1GX2) very closely (79% mode strength and a rmsd of 0.8 Å at R_{tol} = 1.0 Å and 64% mode strength and a rmsd of 0.6 Å at R_{tol} = 0.2 Å) (see Figure 3). Thus, the majority of the docked conformations reproduced the observed complex very well even though they did not have the lowest docking energy.

The crystal structure of the HRP−BHA complex shows that the binding of BHA induces a change in HRP conformation with Phe 68 forming a closed lid over BHA (see Figure 3). Docking to a protein structure showing this conformational change (e.g., 1GX2), rather than the 7ATJ structure that was used, would be expected to reproduce the BHA−HRP complex even better. This protein conformation would, however, probably block MLT and SRT from reaching the heme edge, as these substrates are substantially larger than BHA.

Ferulic acid (FER) is observed experimentally to adopt three alternative conformations (FA1, FA2, and FA3) in the crystal structure of its complex with ferric HRP (*19*). By docking FER to the ferric form of HRP, only FA3 was recovered to a significant extent (20% mode strength at R_{tol} = 1.0 Å and energy at −9.3 kcal/mol). Henriksen and coworkers also determined the structure of the complex of ferric HRP and FER with a cyanide ion bound in the sixth Fe-coordinating position to emulate a nonreactive form of co I (*19*). In this structure, the FA2 and FA3 modes are absent and only the FA1 mode is observed. FER was docked to a target consisting of the protein with a cyanide ion and one structural water molecule added. The best scored mode was not close to any of the experimental positions of FER (48% strength at R_{tol} = 1.0 Å and an energy of −8.4 kcal/mol, rmsd to FA3 = 4.4 Å and to FA1 = 6.3 Å). However, the second best scored docked mode (26% strength at R_{tol} = 1.0 Å and an energy of −7.4 kcal/mol) reproduced FA1 with a rmsd of 0.9 Å, and consistent with the experiment, no docked modes resembled FA2 or FA3 (see Figure 3).

Although the mode strengths were rather low, AUTODOCK was able to reproduce the FA3 and FA1 binding conformations under conditions where they are known to be present and to exclude FA3 under conditions where it is known to be absent. The failure to reproduce FA2 and FA1 in the ferric state HRP may occur because they are located rather far from the active site, and because they have few interactions with HRP itself, structural waters and ions contribute to their binding.

Despite the limitations of the AUTODOCK procedure in neglecting protein flexibility and not being able to automatically account for water molecules mediating ligand−protein

Table 2: Summary of the Results of Docking Melatonin and Serotonin to Horseradish Peroxidase and Myeloperoxidase

	horseradish peroxidase			myeloperoxidase		
oxidation state[a]	orientation of modes[b]	total strength of modes (%)	minimum indole−heme distance (Å)[c]	orientation of modes [b]	total strength of modes (%)	minimum indole−heme distance (Å)[c]
			Melatonin			
F-F	SC	15	6.4	IS	46	3.5
	IS	47	4.1	I	18	3.5
1-1	SC	11	6.5	−	−	−
	IS	58	4.2			
2-2	SC	7	6.2	−	−	−
	IS	58	4.2			
F-1	SC	9	6.3	I	35	3.3
	IS	64	4.2	IS	41	3.5
F-2	SC	7	6.3	I	29	3.4
	IS	60	4.2	IS	43	3.5
			Protonated Serotonin			
F-F	IS	83	4.3	IS	48	3.4
				I	31	3.5
1/F-1	IS	64	4.2	IS	36	3.4
	SC	32	5.1	I	33	3.5
2/F-2	IS	75	4.2	IS	31	3.5
	SC	23	4.6	I	33	3.4
			Unprotonated Serotonin			
F-F	IS	46	4.2	IS	61	3.5
	SC	28	4.1	I	24	3.5
	I	13	4.7			
1/F-1	IS	37	4.2	IS	34	3.4
	SC	61	4.8	I	38	3.5
2/F-2	IS	42	4.2	IS	43	3.4
	SC	56	4.5	I	27	3.5

[a] Oxidation state is denoted with the conformation used first and the chemical/electrostatic assignment second (F for ferric, 1 for compound I, and 2 for compound II). For serotonin, the full representations of co I and co II of HRP are compared with the chemical/electrostatic representations of MPO co I and co II. [b] The modes are described by the part of the ligand that is presented toward the heme Fe ion (IS for indole substituent, SC for side chain, and I for indole aromatic rings). They are listed for each oxidation state with the most energetically favorable first. Details of all docking modes are given in the Supporting Information. [c] The distance from the center of the heme D pyrrole ring to the closest indole atom of the mode.

interactions, the binding mode of BHA and two of the three binding modes of FER to HRP were identified by docking, and this procedure was thus applied to the docking of MLT and SRT.

Docking of Melatonin and Serotonin to Horseradish Peroxidase. SRT (both protonated and unprotonated forms) and MLT were docked to five different targets representing HRP in different reactive states (see Materials and Methods). The five HRP targets were the ferric state, co I and co II crystal structures, and two models of co I and co II derived from the crystal structure of the ferric state. The latter two models were used for comparison with the co I and co II models of MPO for which only crystal structures of the ferric state are available (see the next section). In the models of co I and co II, the crystallographic coordinates of the ferric form were used, a sixth ligand oxygen was added, and the charges were redistributed according to the oxidation state. All docked modes are presented in Table S3 of the Supporting Information. The reproducibility of the docked modes was very good for all the dockings of SRT (83−98% total mode strength) and fair for MLT (62−73%) (see Table 2).

With one exception (the third best scored mode for unprotonated SRT docked to ferric HRP), SRT and MLT did not stack their indole rings to any part of the heme in the docked modes. In general, the indole moiety was docked some distance from the heme edge, with the distance from the closest indole atom to the D pyrrole ring of the heme being 4.1−6.5 Å for MLT and 4.1−5.2 Å for SRT. MLT and SRT were docked in two main orientations in all five different HRP targets (Figure 4). One directs the indole substituent toward the distal cavity (IS modes), and the other directs the ligand side chain toward the distal cavity (SC modes). All the observed docking modes for co I and co II, whether for the crystal structures or for the targets modeled on the basis of the ferric structure, were found in the proximity of the C20 atom, the C18 methyl, and the D ring of the heme.

Docking of Melatonin and Serotonin to Myeloperoxidase. MLT and SRT were docked to three different targets representing MPO in the three reactive states. The MPO targets were the ferric crystal structure and models of co I and co II based on the ferric crystal structure. All resulting modes from these simulations are presented in Table S4 of the Supporting Information. The reproducibility of the docked structures was good for unprotonated SRT (70−85% total mode strength) and fair for protonated SRT (64−79%) and MLT (64−76%) (see Table 2).

Both MLT and SRT could be docked into all forms of the MPO target with their indole rings parallel to the heme plane and close enough to the D pyrrole ring to achieve stacking (Figure 5). The distances of the closest indole atom to the center of the D ring were 3.3−3.5 Å for MLT and 3.4−3.5 Å for both forms of SRT. The ligand side chain was never directed toward the distal cavity. In many cases,

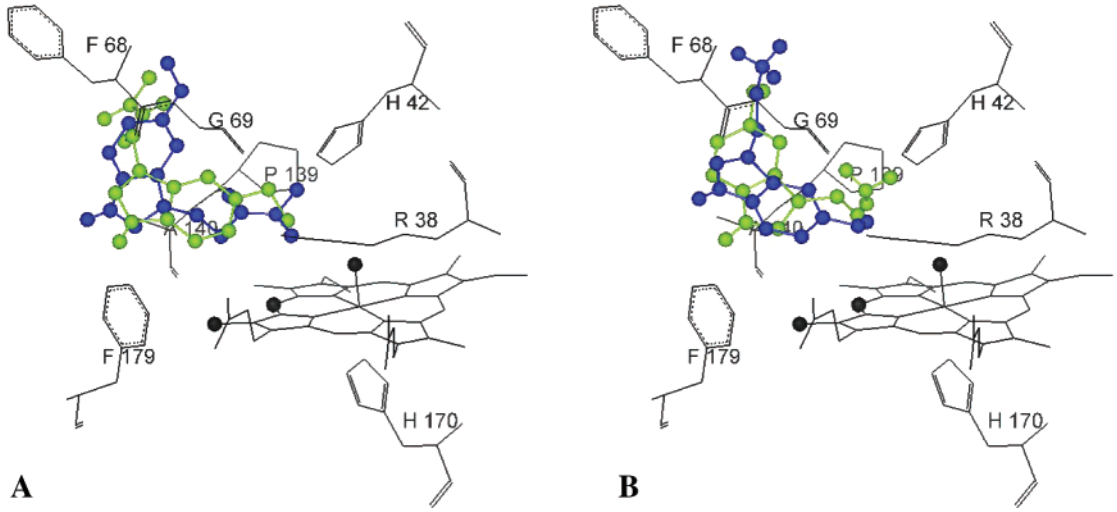

FIGURE 4: Docking modes in the active site of HRP co I. The C18 methyl, C20, and the ferryl oxygen are shown as black balls. (A) For MLT, the docking mode with the best energy score is in the SC (blue) orientation whereas the docking mode with the second best energy score has a higher mode strength and is in the IS (green) orientation. (B) For protonated SRT, the docking mode with the best energy score and highest strength is in the IS (blue) orientation whereas the second best scoring mode is in the SC (green) orientation. Similar docking modes for MLT and SRT are obtained in all five different forms of HRP used for docking.

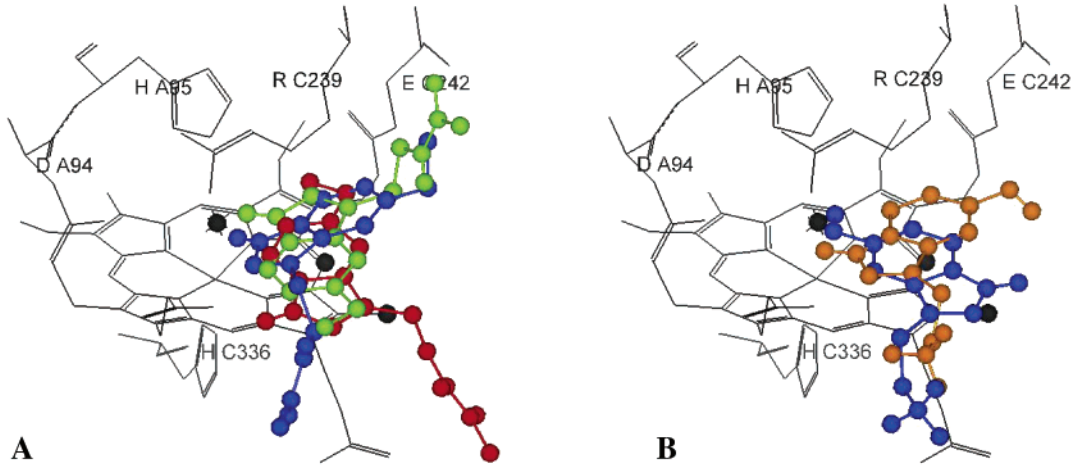

FIGURE 5: Docking modes in the active site of the modeled MPO co I target. The C18 methyl, C20, and the ferryl oxygen are shown as black balls. (A) For MLT, the docking mode with the best energy score is in the I (blue) orientation, the docking mode with the second best energy score and the highest mode strength is in the IS (red) orientation, and the docking mode with the third best energy score and second highest mode strength is in the I (green) orientation. (B) For protonated SRT, the docking mode with the best energy score and highest strength is in the IS (blue) orientation whereas the second best scoring mode is in the I (orange) orientation. All modes found for the co I state of MPO were also observed for MPO co II with the same ranking.

the indole substituent at the 5 position was directed at the distal cavity (IS modes; see Chart 1). The substituent itself was often close to the heme center and the Fe ion. Other modes presented the indole side to the distal cavity (I modes). This orientation created the two possibilities of directing either the side chain or the indole substituent toward a pocket located upward along the periphery of the distal cavity toward Glu C242 (Figure 5). While the docking modes of MLT exploited both possibilities, neither protonated nor unprotonated SRT forms ever directed their side chain toward this pocket.

DISCUSSION

Comparison of Docked Complexes in HRP and MPO. Figure 6 shows the docking modes obtained in both HRP and MPO. The docking modes can be distinguished by which part of the ligand docks closest to the heme as IS (indole substitutent), I (Indole ring), or SC (side chain).

All the docking modes of MLT and SRT in co I and co II are consistent with the idea that the heme edge near the D ring and C20 form the site of peroxidase reduction in reactions 2 and 3 in both enzymes. Only the docked modes for the ferric state could penetrate further into the distal cavity. In this comparison, however, we will only consider dockings to co I and co II for which MLT and SRT are substrates. While the site of heme interactions is common to HRP and MPO, the similarities between HRP and MPO dockings end here.

First, the modes docked into MPO have a closer interaction with the heme edge and especially with the D ring (Figure 6). The mean measured distances from the center of the D ring to the closest indole atom of the mode are 0.9−1.2 Å shorter for docking modes in MPO than in HRP (see Table 2). Second, for any ligand, the equivalent docking modes in MPO systematically have docking free energies that are slightly more favorable than those in HRP (Tables S3 and

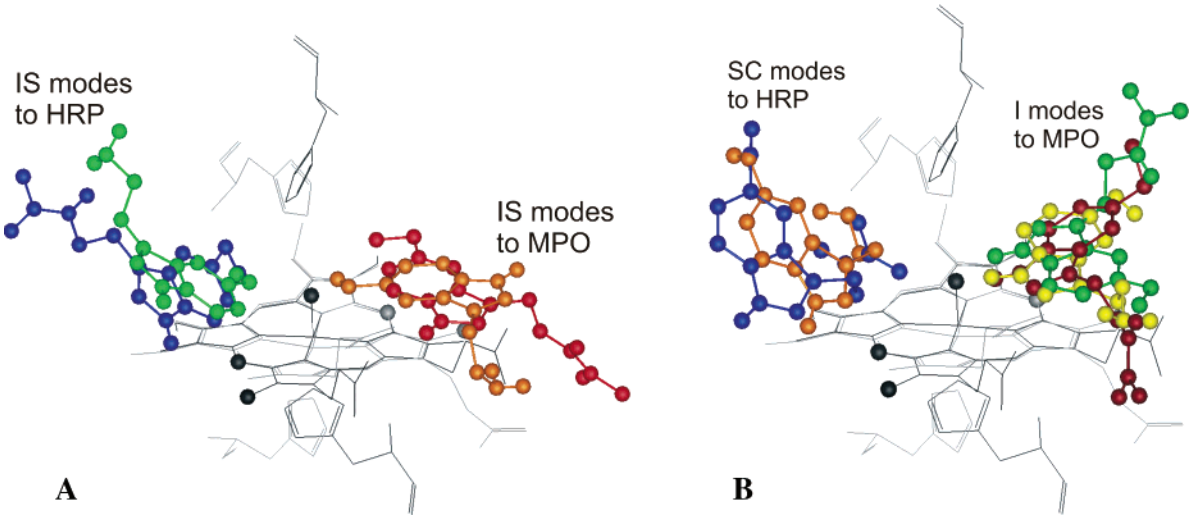

FIGURE 6: Superposition of the active sites of the co I states of HRP (black) and MPO (gray) showing docking modes of MLT and SRT. The hemes and proximal and distal histidines of the active sites are shown. The C18 methyl, C20, and the ferryl oxygen are shown as balls (black for HRP and gray for MPO). The docking modes shown orient their indole substituent (IS) inward (A) or their indole side (I) or side chain (SC) inward (B). The modes of docking to HRP are on the left side of the figures, and the modes of docking to MPO are on the right side of the figures (corresponding to the channel locations in the two proteins). For HRP, modes are shown for MLT [blue (A and B)] and unprotonated SRT [green (A) and orange (B)]. For MPO, modes are shown for MLT [red (A and B) and green (B)] and unprotonated SRT [orange (A) and yellow (B)].

S4). Third, all the docking modes in MPO are potentially able to engage in aromatic stacking with the D ring of the heme (Table S4). None of the docking modes in HRP is able to do so because their indole rings are too far from the heme edge and are not parallel to the heme plane. Fourth, all docking modes in MPO have the ligand side chain oriented away from the Fe ion and offer the indole possibilities for close interaction with the heme. In contrast, the SC modes for MLT in HRP (Figure 6) point the bulky ligand side chain into the active site, thus pushing the central indole more than 5 Å from the center of the D ring. This observation supports the notion that the indole substituent or the indole itself is more important to the reaction than the substrate side chain. Indeed, in the reduction of HRP by the auxin, indoleacetic acid, an indole electron was found to be transferred (*1*, *30*). In all, these observations are consistent with the rate constants of MPO being higher than those of HRP (Table 1). However, the ratios of the rate constants for MPO and HRP differ (over a range from 1.2 to 400) for the k_2 and k_3 rate constants for SRT and MLT (Table 1). This difference cannot be explained quantitatively by the docking results as neither the HRP nor the MPO co II docking patterns differed significantly from those in co I.

Comparison of Docked Complexes of Melatonin and Serotonin. The substituent of the central indole has been suggested to have the most important role in electron transfer in reactions 2 and 3. Correlation with the Hammett σ coefficients of peroxidase substrates shows that the presence of electron-donating groups, such as methoxy and hydroxyl groups, as aromatic ring substituents increases reaction rates (*1*, *29*). Alterations in the functional groups in the ligand side chain have a weaker effect on reaction rates (*12*). This is consistent with the reaction mechanism known for indoleacetic acid (*30*) and the identification of docking modes (IS modes) with the indole substituent pointing to the active site in HRP and MPO.

The IS modes are generally the dominant ones with respect to mode strength (see Table 2). The IS modes of MLT and SRT are fairly similar with regard to the position of the indole (Figure 6A). The shortest distance from the indole to the center of the D ring is approximately 4.1−4.6 Å for MLT and 4.2 Å for SRT in HRP, but only 3.4−3.5 Å for both substrates in MPO. The indole substituent of SRT docks approximately 1 Å closer to the heme edge than that of MLT (see Figure 6A). The greatest difference between MLT and SRT IS mode dockings is that in MPO, MLT is flipped over by 180° in comparison with SRT. This is probably because the methoxy group of MLT is too large to be directed straight into the distal cavity like the smaller hydroxyl group of SRT.

In the SC modes of MLT in HRP, the bulky MLT side chain forces the indole ring away from the heme edge, resulting in indole−D ring center distances of 6.2−6.5 Å. In contrast, the SC modes of SRT have indole−D ring center distances of 4.5−5.2 Å, similar to those of the IS modes. This implies that MLT is less likely to be in the active site with its indole close to the heme edge than SRT.

The I modes of MLT and SRT in MPO (Figure 6B) appear to have the central indole in the same place. MLT has somewhat fewer stacking possibilities than SRT, but no significant differences are observed otherwise. The indole−D ring distances are 3.3−3.5 Å for MLT and 3.4−3.5 Å for SRT. The orientation of the side chain constitutes the largest difference between MLT and SRT modes of docking to MPO. In addition to having its side chain point out into the access channel like SRT, MLT has its rather large side chain pointing into a pocket along the periphery of the distal cavity (Figure 6B, green mode).

MLT and SRT indoles are found with the same distances to the heme edge regardless of the mode of docking in MPO. But in HRP, the indole substituent of MLT is located farther from the heme edge than that of SRT, and MLT displays

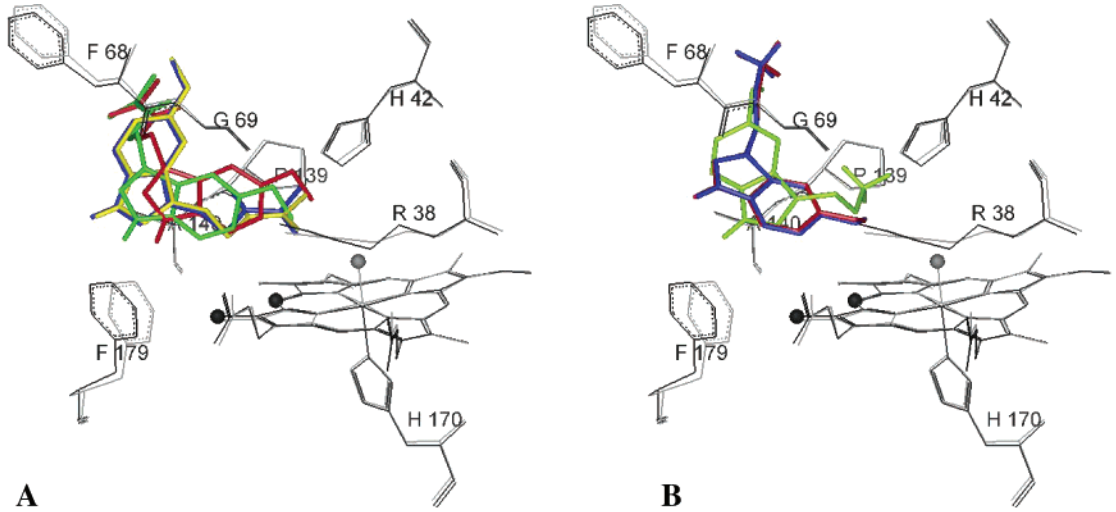

FIGURE 7: Superposition of the HRP ferric (black) and co I (gray) active sites showing docking modes. The C18 methyl, C20, and the ferryl oxygen are shown as balls in the color of the respective HRP state. (A) For MLT, the SC mode in ferric (yellow) and co I (blue) states and the main IS mode in ferric (red) and co I (green) states are shown. (B) For protonated SRT, the IS mode in ferric HRP (red) (the only mode found for this state) and in co I (blue) and the SC mode (green) found only in the HRP co I state are shown, although for unprotonated SRT, a similar SC mode was also found in the ferric state.

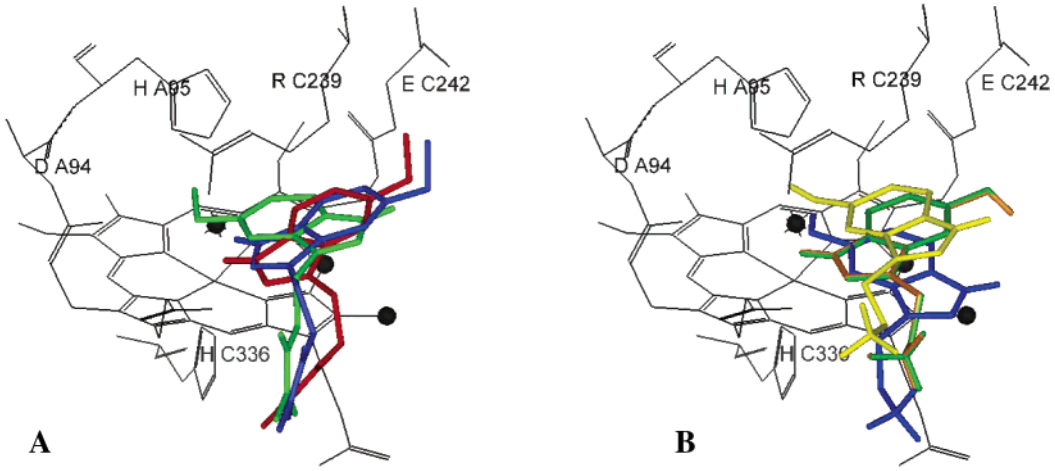

FIGURE 8: Structure of ferric MPO with a ferryl oxygen added to emulate MPO co I. The C18 methyl, C20, and the ferryl oxygen are represented as black balls. (A) For MLT, the most energetically favorable IS mode, found only in ferric MPO (green), and the most energetically favorable I mode found in both the ferric (red) and the emulated co I (blue) and co II states are shown. (B) For protonated SRT, the IS mode found only in ferric state MPO (yellow), the IS mode found only in the emulated co I (blue) and co II states, and the I mode found in the ferric (green) and the emulated co I (orange) and co II states are shown.

significant distance differences, depending on the docking mode. This could therefore explain why the ratio of the SRT to MLT k_2 rate constants of HRP co I (620) could be so much greater than that of MPO co I (2.8).

This phenomenon of a greater substrate specificity of HRP than of MPO is not confined to SRT and MLT but has been observed for a variety of other indoles (*12*). However, this still does not explain why the rate constants of MPO co II are so much smaller than those of MPO co I or why the substrate specificity of MPO co II would be at the same levels as that of HRP co II while being rather unspecific in co I. The ratio of the SRT to MLT k_3 rate constants in HRP and MPO co II is 2300 and 1500, respectively.

Comparison of Dockings to the Oxidation States of Peroxidase: Ferric vs Compounds I and II. In HRP, the SC mode for MLT is largely unaffected by the differences between ferric and co I and II states, whereas the main IS mode is pushed ~1 Å away from the ferryl oxygen (Figure 7). For SRT, on the other hand, the IS mode is unaffected, whereas the SC mode is absent (protonated SRT) or much weaker (unprotonated SRT) in the ferric state than in the co I and II states. Apart from these differences, which all stem from the presence or absence of the ferryl oxygen, the positions of docking of the substrates to HRP in the three oxidation states are rather similar. This pattern was also observed in the GRID maps (see Results). This suggests that structural models of substrate−ferric HRP complexes should be fairly reliable indicators of the substrate docking position for co I or II.

In MPO, all modes found in the co I state were also observed in co II. However, when the ferric and co I and II states of MPO were compared, both MLT and SRT were again pushed ~1 Å away from the ferryl oxygen (Figure 8). The most energetically favorable IS mode for MLT (Figure 8A, green) was found in the MPO ferric state and directs the MLT methoxy group directly into the distal cavity. The distance of the methoxy oxygen to the Fe ion is 2.9 Å. This mode is abolished when the ferryl oxygen is added, restrict-

ing MLT IS mode docking positions to the flipped-over IS mode shown in Figure 5. Similarly, the most energetically favorable SRT IS modes in the ferric state (Figure 8B, yellow), with a 3.0 Å distance from the hydroxyl oxygen to the Fe ion, were also abolished in co I and II. SRT was however able to point the hydroxyl group directly into the distal cavity by using a "pushed-out" IS mode, not found in the ferric state (Figure 8B, blue). The I modes for both substrates are very similar in the ferric and co I and II states of MPO.

These observations highlight another consequence of MPO having a more spacious active site than HRP. In the MPO ferric state, the indole substituents penetrate to within 3 Å of the Fe ion. In HRP, no indole substituents docked within 4.0 Å of the Fe ion. Electrostatic differences aside, the ferryl oxygen is the only addition made to the MPO ferric structure to represent co I. Thus, the ferryl oxygen in MPO co I enforces a substrate docking pattern different from that of the ferric state. In contrast, the ferric HRP structure does not allow the substrate to move close enough to experience the energetic and steric differences originating from the presence or absence of the ferryl oxygen. The small differences in docking observed in HRP could also be caused by other conformational movements (e.g., of the distal His 170, Arg 38, or Phe 179) or by differences in charge distribution. This indicates that even if models of substrate−ferric HRP complexes are fairly reliable for emulating docking of the substrate to co I or II, modeled substrate−ferric MPO complexes are probably not. This is especially so, as possible conformational changes of MPO during reaction 1 or 2 have not been elucidated crystallographically.

Comparison of Dockings to the Oxidation States of Peroxidase: Compound I vs Compound II. In HRP, the IS modes have the greatest mode strength for MLT and only small conformational and positional differences were detected between the different IS modes in co I and co II (Figure S1). This is not surprising as the structural differences between HRP co I and co II active sites are very small. However, the relative strengths of the different IS modes differ between co I and co II. The SC mode for MLT is almost unaffected by the difference between co I and co II. The SC modes of SRT show small shifts of 0.3−0.4 Å between co I and co II but are not as sensitive to the heme protein differences as the IS modes of MLT.

Importantly though, models of HRP co I and co II based on the ferric structure (F-1 and F-2, respectively, in Table 2) did not reproduce these shifts between co I and co II (Figure S2). Moreover, the comparison between co I and co II dockings in MPO, which assume that no structural changes take place in the protein, did not reveal any significant differences (>0.2 Å) in docked positions at all. Therefore, it may be assumed that conformational differences in the protein, albeit small, still exert a stronger influence over the substrate docking pattern than the chemical/electrostatic changes between co I and co II.

The docking results for MPO co I and co II do not explain the large difference between k_2 and k_3 rate constants in MPO and cannot explain the higher substrate specificity of co II either. Single-electron reduction potential measurements (*14*) (Table 1) have produced values that agree with the relative differences observed, but the reduction potential values in turn depend on other properties such as structure. When put together, these observations further strengthen the proposal of a conformational or polarizational change taking place during reaction 2 or 3 in MPO. It is possible that, as the IS docking modes of SRT and MLT differ in orientation from each other, a conformational or electrostatic change in the macromolecule could affect SRT and MLT reactivity quite differently. As the experimental measurements and docking results are compatible for MPO co I, a conformational change in reaction 3 appears more probable than in reaction 2.

Limitations and Sources of Error. Apart from the mentioned lack of experimental structures of MPO co I and co II, the limitations and sources of error were investigated in the validation docking experiments. Notable limitations are the assumption of a rigid macromolecule in AUTODOCK where amino acid residues of the peroxidase are not permitted to move and so cannot interact with the substrate in a flexible way. Another limitation is that the docking procedure does not account for water molecules that may participate in the binding of the substrates or in the redox reactions.

CONCLUSIONS

In both HRP and MPO, all docking modes show the aromatic substrates close to the heme edge containing C20 and the D pyrrole ring, consistent with this part of the heme being the site of reduction of the peroxidase by the substrate. The docking calculations also show the indole substituent and/or the indole ring moieties of the substrate positioned at the heme edge, and this is consistent with these moieties having a stronger influence over the rates of reactions 2 and 3 (Figure 1) than ligand side chain substituents (Chart 1). Despite the common docking site with respect to the heme, the differences in the docking orientation and the differences in the shape and size of the active sites and their access channels provide explanations for some of the observed differences in specificity and catalysis of indole derivatives by HRP and MPO.

(1) The heme edge is more accessible in MPO than in HRP, resulting in docked modes of MLT and SRT in MPO that are closer to the heme edge than the corresponding modes in HRP. Some of the modes in MPO display ring stacking between the indole rings and the heme D ring, which may contribute to the reduction rates of MPO co I and co II being higher than those of HRP.

(2) The greater proximity to the heme edge in HRP of the docked SRT compared to MLT results in a shorter electron transfer distance. This is consistent with the observed higher k_2 and k_3 rate constants in HRP for SRT compared to those for MLT.

(3) The greater active site access restriction in HRP than in MPO, and the observation that the only advantage SRT has over MLT in MPO co I and co II is the ability of one major SRT mode to point the indole substituent directly into the distal cavity, demonstrate factors contributing to the greater substrate specificity of HRP co I compared to MPO.

(4) The small structural differences between HRP ferric, co I, and co II forms have a greater impact on docking mode than the addition of the ferryl oxygen or electrostatic changes in HRP. This is consistent with the specificity of HRP being greater for MLT, which is larger than SRT.

(5) No significant differences in the docking mode were observed between the chemical/electrostatic representations

of MPO co I and co II. Thus, while the docking study provides explanations for differences in k_2 rate constants between MPO and HRP, it does not explain the relative differences in k_3 rate constants between MPO and HRP. Measured redox potentials are consistent with these relative differences, but the structural basis for the differences in redox potentials remains to be revealed. To obtain a deeper understanding of the determinants of the reaction rates of these enzymes, a better knowledge of the structures and charge distributions of MPO co I and co II is needed.

ACKNOWLEDGMENT

We thank Prof. Lars Olsen and Prof. Janos Hajdu for useful discussions and Dr. Peter J. Winn and Dr. Matthias Stein for critical reading of the manuscript.

SUPPORTING INFORMATION AVAILABLE

Heme charge derivation procedures, partial atomic charges assigned to hemes, partial atomic charges assigned to indole substrates, and details of docking modes. This material is available free of charge via the Internet at http://pubs.acs.org.

REFERENCES

1. Dunford, H. B. (1999) *Heme Peroxidases*, Wiley, New York.
2. Veitch, N. C. (2004) Horseradish peroxidase: A modern view of a classic enzyme, *Phytochemistry 65*, 249−259.
3. Klebanoff, S. J. (2005) Myeloperoxidase: Friend and foe, *J. Leukocyte Biol. 77*, 598−625.
4. Fiedler, T. J., Davey, C. A., and Fenna, R. E. (2000) X-ray crystal structure and characterization of halide-binding sites of human myeloperoxidase at 1.8 Å resolution, *J. Biol. Chem. 275*, 11964−11971.
5. Hoy, A., Leininger-Muller, B., Kutter, D., Siest, G., and Visvikis, S. (2002) Growing significance of myeloperoxidase in non-infectious diseases, *Clin. Chem. Lab. Med. 40*, 2−8.
6. Tafazoli, S., and O'Brien, P. J. (2005) Peroxidases: A role in the metabolism and side effects of drugs, *Drug Discovery Today 10*, 617−625.
7. Silva, S. O., Ximenes, V. F., Catalani, L. H., and Campa, A. (2000) Myeloperoxidase-catalyzed oxidation of melatonin by activated neutrophils, *Biochem. Biophys. Res. Commun. 279*, 657−662.
8. Allegra, M., Furtmüller, P. G., Regelsberger, G., Turco-Liveri, M. L., Tesoriere, L., Perretti, M., Livrea, M. A., and Obinger, C. (2001) Mechansim of Reaction of Melatonin with Human Myeloperoxidase, *Biochem. Biophys. Res. Commun. 282*, 380−386.
9. Silva, S. O., Rodrigues, M. R., Carvalho, S. R., Catalani, L. H., Campa, A., and Ximenes, V. F. (2004) Oxidation of melatonin and its catabolites, N1-acetyl-N2-formyl-5-methoxykynuramine and N1-acetyl-5-methoxykynuramine, by activated leukocytes, *J. Pineal Res. 37*, 171−175.
10. Olsen, L. F., Kummer, U., Kindelzkii, A. L., and Petty, H. R. (2003) A Model of the Oscillatory Metabolism of Activated Neutrophils, *Biophys. J. 84*, 69−81.
11. Gabdoulline, R. R., Kummer, U., Olsen, L. F., and Wade, R. C. (2003) Concerted Simulations Reveal How Peroxidase Compound III Formation Results in Cellular Oscillations, *Biophys. J. 85*, 1421−1428.
12. Jantschko, W., Furtmüller, P. G., Allegra, M., Livrea, M. A., Jakopitsch, C., Regelsberger, G., and Obinger, C. (2002) Redox Intermediates of Plant and Mammalian Peroxidases: A Comparative Transient-Kinetic Study of Their Reactivity Toward Indole Derivatives, *Arch. Biochem. Biophys. 398*, 12−22.
13. Ximenes, V. F., Catalani, L. H., and Campa, A. (2001) Oxidation of melatonin and tryptophan by an HRP cycle involving compound III, *Biochem. Biophys. Res. Commun. 287*, 130−134.
14. Jantschko, W., Furtmüller, P. G., Zederbauer, M., Neugschwandtner, K., Lehner, I., Jakopitsch, C., Arnhold, J., and Obinger, C. (2005) Exploitation of the unusual thermodynamic properties of human myeloperoxidase in inhibitor design, *Biochem. Pharmacol. 69*, 1149−1157.
15. Furtmüller, P. G., Arnhold, J., Jantschko, W., Pichler, H., and Obinger, C. (2003) Redox properties of the couples compound I/compound II and compound II/native enzyme of human myeloperoxidase, *Biochem. Biophys. Res. Commun. 301*, 551−557.
16. Farhangrazi, Z. S., Fossett, M. E., Powers, L. S., and Ellis, W. R., Jr. (1995) Variable temperature spectroelectrochemical study of horseradish peroxidase, *Biochemistry 34*, 2866−2871.
17. Dunford, H. B., and Hsuanyu, Y. (1999) Kinetics of oxidation of serotonin by myeloperoxidase compounds I and II, *Biochem. Cell Biol. 77*, 449−457.
18. Sarada, B. V., Rao, T. N., Tryk, D. A., and Fujishima, A. (2000) Electrochemical oxidation of histamine and serotonin at highly boron-doped diamond electrodes, *Anal. Chem. 72*, 1632−1638.
19. Henriksen, A., Smith, A. T., and Gajhede, M. (1999) The Structures of the Horseradish Peroxidase C−Ferulic Acid Complex and the Ternary Complex with Cyanide Suggest How Peroxidases Oxidize Small Phenolic Substrates, *J. Biol. Chem. 274*, 35005−35011.
20. Berglund, G. I., Carlsson, G. H., Smith, A. T., Szöke, H., Henriksen, A., and Hajdu, J. (2002) The catalytic pathway of horseradish peroxidase at high resolution, *Nature 417*, 463−468.
21. Goodford, P. J. (1985) A computational procedure for determining energetically favorable binding sites on biologically important macromolecules, *J. Med. Chem. 28*, 849−857.
22. Banci, L., Carloni, P., and Savellini, G. G. (1994) Molecular dynamics studies on peroxidases: A structural model for horseradish peroxidase and a substrate adduct, *Biochemistry 33*, 12356−12366.
23. Morris, G. M., Goodsell, D. S., Halliday, R. S., Huey, R., Hart, W. E., Belew, R. K., and Olson, A. J. (1998) Automated Docking Using a Lamarckian Genetic Algorithm and Empirical Binding Free Energy Function, *J. Comput. Chem. 19*, 1639−1662.
24. Vriend, G. (1990) WHAT IF: A molecular modeling and drug design program, *J. Mol. Graphics 8*, 52−56.
25. Ghosh, A., Almlöf, J., and Que, L. (1994) Density Functional Theoretical Study of Oxo(porphyrinato)iron(IV) Complexes, Models of Peroxidase Compounds I and II, *J. Phys. Chem. 98*, 5576−5579.
26. Poulos, T. L., and Kraut, J. (1980) The Stereochemistry of Peroxidase Catalysis, *J. Biol. Chem. 255*, 8199−8205.
27. Wirstam, M., Blomberg, M. R. A., and Siegbahn, P. E. M. (1999) Reaction Mechanism of Compound I Formation in Heme Peroxidases: A Density Functional Theory, *J. Am. Chem. Soc. 121*, 10178−10185.
28. Henriksen, A., Schuller, D. J., Meno, K., Welinder, K. G., Smith, A. T., and Gajhede, M. (1998) Structural Interactions between Horseradish Peroxidase C and the Substrate Benzhydroxamic Acid Determined by X-ray Crystallography, *Biochemistry 37*, 8054−8060.
29. Sakurada, J., Sekiguchi, R., Sato, K., and Hosoya, T. (1990) Kinetic and Molecular Orbital Studies on the Rate of Oxidation of Monosubstituted Phenols and Anilines by Horseradish Peroxidase Compound II, *Biochemistry 29*, 4093−4098.
30. Candeias, L. P., Folkes, L. K., Menuchehr, P., Parrick, J., and Wardman, P. (1996) Rates of Reaction of Indoleacetic Acids with Horseradish Peroxidase Compound I and Their Dependence on the Redox Potentials, *Biochemistry 35*, 102−108.
31. MacKerell, A. D., Bashford, D., Bellott, M., Dunbrack, R. L., Evanseck, J. D., Field, M. J., Fischer, S., Gao, J., Guo, H., Ha, S., Joseph-McCarthy, D., Kuchnir, L., Kuczera, K., Lau, F. T. K., Mattos, C., Michnick, S., Ngo, T., Nguyen, D. T., Prodhom, B., Reiher, W. E., Roux, B., Schlenkrich, M., Smith, J. C., Stote, R., Straub, J., Watanabe, M., Wiorkiewicz-Kuczera, J., Yin, D., and Karplus, M. (1998) All-Atom Empirical Potential for Molecular Modeling and Dynamics Studies of Proteins, *J. Phys. Chem. B 102*, 3586−3616.
32. Blair-Johnson, M., Fiedler, T., and Fenna, R. (2001) Human myeloperoxidase: Structure of a cyanide complex and its interaction with bromide and thiocyanate substrates at 1.9 Å resolution, *Biochemistry 40*, 13990−13997.
33. Binkowski, T. A., Naghibzadeh, S., and Liang, J. (2003) CASTp: Computed Atlas of Surface Topography of proteins, *Nucleic Acids Res. 31*, 3352−3355.
34. Taylor, R. D., Jewsbury, P. J., and Essex, J. W. (2002) A review of protein-small molecule docking methods, *J. Comput.-Aided Mol. Des. 16*, 151−166.

BI051510E